Journal of Molecular Liquids 395 (2024) 123933

Contents lists available at ScienceDirect

Journal of Molecular Liquids

journal homepage: www.elsevier.com/locate/molliq

Preparation and characterization of stable methyl myristate−in−water nanoemulsions as advanced working fluids for cooling systems

D. Cabaleiro [a,*], C. Hermida−Merino [a], S. Losada−Barreiro [b], F. Agresti [c], L. Lugo [a], D. Hermida−Merino [a], M.M. Piñeiro [a,*]

[a] Departamento de Física Aplicada, Universidade de Vigo, E−36310 Vigo, Spain
[b] Departamento de Química−Física, Universidade de Vigo, E−36310 Vigo, Spain
[c] CNR ICMATE, Corso Stati Uniti 4, I−35127 Padova, Italy

ARTICLE INFO

Keywords:
Phase change material emulsion (PCME)
Fatty acid methyl ester (FAME)
Nanoemulsion optimization
Thermophysical properties
Heat storage capacity
Subcooling
Rheological behavior

ABSTRACT

Phase change material emulsions (PCME) have gained increasing scientific interest due to their potential to enhance the storage capability of thermal facilities. Herein we present the design and characterization of oil−in−water (O/W) nanoemulsions by employing a dispersed phase mixture (2–12 wt%) enriched in methyl myristate as phase change material. The emulsifier and dispersed phase compositions were optimized based on dynamic light scattering and calorimetric analyses. A two−surfactant formulation composed of sodium dodecyl sulfate and Brij^{TM} S2 (20:49 in weight) was selected to produce stable colloidal dispersions of a methyl stearate: *n*–hexadecane:methyl myristate mixture (at a mass proportion of 1:3:36) in water. No phase separation or significant growth in emulsified droplet size was detected under storage conditions or when the slurries were subjected to different heating−cooling cycles. The melting/crystallization transitions, rheological behavior, thermal conductivity and density of optimized nanoemulsions were experimentally investigated in order to further understand how the concentration and physical state of suspended droplets may influence those thermal and physical properties. According to differential scanning calorimetry studies, slurries showed moderate subcooling degrees (~3 °C), even though their solid−liquid transitions extended over a slightly wider range of temperatures than the same mixture used as the dispersed phase but in bulk−form. The shear−thinning character observed for developed nanoemulsions at low temperatures disappeared with the melting of suspended droplets. Considering an operating temperature interval of 15 °C around melting−crystallization phase changes, the 12 wt % optimized suspension presented a storage capacity 18 % higher than that of water under the same conditions. Furthermore, thermal reliability tests verified that phase change characteristics did not significantly changed after 8 months of storage and throughout 500 thermal cycles.

1. Introduction

Growth in worldwide energy consumption and environmental degradation are unequivocally recognized as two of the most pressing issues facing our societies today [1]. In this scenario, building stock is a major contributor, accounting for 40 % of the total final energy demand and 36 % of anthropogenic CO_2 emissions in the European Union [2]. Owing to the important energy−saving potential lying in this sector, significant efforts have been made to integrate renewables and improve efficiency, particularly in heating, ventilation, and air conditioning facilities. In this regard, thermal energy storage (TES) strategies based on phase change materials (PCMs) have become a relevant research topic in recent years [3]. PCMs use the latent heat involved in a phase change, usually a solid−liquid or solid−solid transition, to leverage large amounts of thermal energy at nearly isothermal conditions [4]. However, large−scale use of PCMs in thermal facilities still requires increasing their flexibility by overcoming certain technical issues such as the low thermal conductivity or leakage as well as further working on their implementation [5,6]. More specifically, bulk−PCMs cannot flow when they are in solid phase. As a consequence, a secondary carrier fluid and a heat exchanger are usually necessary to transport the stored/retrieved thermal energy to where demand exists [7]. In order to reduce the cost and improve the compactness factor of the TES system, an interesting alternative is to conjugate both the phase change material

* Corresponding authors.
E-mail addresses: dacabaleiro@uvigo.es (D. Cabaleiro), mmpineiro@uvigo.es (M.M. Piñeiro).

https://doi.org/10.1016/j.molliq.2023.123933
Received 26 September 2023; Received in revised form 19 December 2023; Accepted 28 December 2023
Available online 2 January 2024

and carrier fluid to formulate a PCM slurry. The idea is to integrate in just one medium the good transport properties of a conventional heat transfer fluid and the larger storage capacity of a phase change process [8,9].

Among the different types of two−phase slurries, phase change material emulsions (PCMEs) are potentially attractive heat transfer and storage media for a wide range of applications including solar harvesting [10,11] electronics [12,13] or HVAC systems [14–16]. In this type of latent functional fluids, the PCM (dispersed phase) is suspended in an immiscible carrier fluid (continuous phase) as fine droplets with the assistance of appropriate surfactants [17,18]. PCMEs offer certain advantages such as relatively−simple technical preparation, reduced large−scale production costs, fluid−like appearance (regardless the solid/liquid state of PCM droplets) and nearly negligible thermal resistance between PCM and CF components [19,20]. Additionally, when dispersed droplets are in nano−metric scale, it is possible to obtain large specific surface areas between dispersed and continuous phases, which further improves the charge and discharge dynamics of the thermal energy absorbed/released by the phase change material [21,22].

In addition to large energy storage capacities at appropriate temperatures, the practical implementation of PCMEs also requires a long lifespan and low pumping power consumption [23,24]. Therefore, significant attempts have been made to achieve small droplet sizes, strong emulsion stabilities and appropriate apparent viscosities. As an example, Liu et al. [10] used a response surface methodology to assess and optimize three key factors in ultrasouns−assisted emulsification (namely surfactant content, treatment time and ultrasound amplitude) when preparing OP18E−in−water nanoemulsions stabilized with a mixture of two non−ionic surfactants (Brij^{TM} L4 and Cremophor®A25). Emulsion composition was identified as the most influential variable, followed by ultrasounds amplitude and treatment time. Predicted results were validated by means of experiments and colloidal suspensions presented fine droplets with average diameters of ~ 124 nm and relatively−low apparent viscosities of ~ 7.3 mPa·s. Wang et al. [25] developed aqueous slurries containing 20 wt% of a paraffin (melting point at 62–64 °C) and stabilized with a mixed polymeric emulsifier consisting of polyethylene glycol (PEG 600) and polyvinyl alcohol (PVA−110 k). In order to define the optimal formulation parameters, the authors systematically explored the influence of PVA−to−PEG mass ratio, the emulsifier−to−paraffin mass ratio and the homogenization shear rate on the size distribution, viscosity and dispersion stability of final PCMEs. In addition, Zhang et al. [26] investigated the effects of surfactant concentration and type (including nine different binary mixtures of Spans and Tweens) as well as emulsification conditions (such as homogenizer type and its operating procedure) on droplet size distribution, emulsion stability and apparent viscosity. Results showed that creaming rate and gravitationally−induced agglomeration and coalescence reduced with rising surfactant concentration and increasing rotation speed. However, these effects strongly relied on the corresponding surfactant mixture.

When materials are confined in narrow spaces such as microcapsules or fine droplets, it is quite unlikely that unintentionally all isolated particles contain non−homogeneities, defects or impurities [27,28]. Consequently, in most phase change material slurries the crystallization of dispersed PCM is mainly governed by homogenous nucleation and, therefore samples typically exhibit considerable subcooling or supercooling degrees (*i.e.* liquid−solid transition upon cooling starts at a lower temperature than melting). Huang et al. [29] and Günther et al. [30] comprehensively investigated the subcooling of *n*–hexadecane−in−water (nano−)emulsions stabilized with various surfactants. The authors observed that subcooling degree reached ~ 12 °C for droplets emulsified by sodium dodecyl sulfate (SDS) and ~ 8 °C for those formulated with polyoxyethylene sorbitan monopalmitate (Tween 40). Since this undesirable phenomenon may hamper the development and application of PCMEs, numerous attempts have been reported in the literature to promote the heterogeneous nucleation during the crystallization of suspended particles [31,32]. The most common strategies involve the addition of nucleation agents, such as PCMs with high−melting points, secondary co−surfactants or solid nanoparticles. Morimoto et al. [33] proved the potential of a high−melting−point fat (glycerol monostearate) to reduce the supercooling degree of *n*–hexadecane−in−water emulsions to only 3 °C. The presence of the fat shell also improved the latent heat stored by dispersed PCM droplets, which authors attributed to a change in paraffin crystallinity at the interface of the *n*–hexadecane−glycerol monostearate shell. Liu et al. [34] prepared *n*–hexadecane−in−water slurries stabilized with Brij^{TM} L4 as primary emulsifier and either polyethylene−block−polyethylene glycol (PE−b−PEG) with a molar weight of 2500 g/mol or polyoxyethylene sorbitan monopalmitate (Tween 60) as co−surfactants. The authors used different contents of *n*–octacosane as nucleating agent and evidenced the positive effect of both the polymeric surfactant PE−b−PEG and *n*–octacosane to lower the supercooling degree of prepared suspensions. Sakai et al. [35] formulated *n*–hexadecane−in−water slurries stabilized by 15 different ionic and non−ionic surfactants. Results revealed that a polyethylene−block−polyethylene glycol (E15EO40) with a long hydrocarbon chain in its hydrophobic moiety was the most effective one to prevent the subcooling of prepared emulsions. Hagelstein and Gschwander [36] analyzed the connections between surfactant type (Span 60, Tween 60, Triton X100 and polyvinyl alcohols, PVA, with different molecular weights) and the subcooling degree of *n*–octadecane−in−water slurries. Calorimetric analyses proved the potential of polyvinyl alcohols to reduce the subcooling of paraffin droplets from 12 °C down to 2 °C. Regarding solid particles, hydrophobic nano−silica [37,38] or several carbon nanostructures [39,40] have been tested as nucleating agents. Zhang et al. [41] prepared aqueous (nano−) emulsions loaded with 30 wt% of *n*–hexadecane and demonstrated that subcooling degree could be suppressed by incorporating 1 wt% hydrophobic SiO_2 nanoparticles to the disperse phase. Barison et al. [39] investigated the influence of graphene oxide and reduced graphene oxide on the subcooling of paraffin−in−water nanoemulsions loaded with either commercial Rubitherm® RT21HC or RT55. Likewise, Zhao et al. [42] developed graphene oxide−Pickering emulsions containing 10 wt% of a paraffin melting at 42–44 °C. The authors observed that carbon nanostructures with adequate amphiphilic nature may be potentially interesting to: *i)* improve suspension stability, *ii)* reduce the subcooling of dispersed droplets, *iii)* increase the thermal conductivity of the final slurry and/or *iv)* enhance optical properties and harvesting of solar radiation.

Hitherto, most investigations on PCM (nano−)emulsions have used *n*–alkanes (so−called paraffins) as dispersed phase [43–45]. These saturated straight−chain hydrocarbons are so−far inexpensive, exhibit high latent heats and are available in an extensive range of phase change temperatures (depending on the number of carbons in their structure) [46]. However, paraffins are usually produced from crude oil distillation in petrochemical refineries and the environmental impact of their manufacturing cannot be overlooked [47]. Thus, the analyses of technical−grade paraffins or discards reveal the presence of some hazardous components such as trichloroethylene, toluene or a wide range of alkenes with unknown health effects and safety [48]. In addition to their non−renewable origin, an increase in their economic cost is expected due to the depletion of petroleum reserves. As a consequence, the development of green phase change materials has gained increasing attention. Bio−based alternatives such as fatty acids, esters or alcohols are mainly obtained from sustainable vegetable oils or animal fats [49]. They exhibit phase change characteristics similar to those of petrol−derivatives while they are less toxic than *n*–alkanes [50]. In fact, most of those bio−based PCM are completely biodegradable and can be considered *"food grade"*, which makes them ideal substitutes in applications where there may be some risk of accidental ingestion [51]. When it comes to PCM (nano−)emulsions, non−paraffinic options are still relatively unexplored. Puupponen et al. [46] formulated fatty acid−in−water nanoemulsions via a phase inversion composition method.

Colloidal suspensions were loaded with 1–5 % contents of stearic acid as dispersed phase and stabilized with different mixtures of SDS, sorbitan trioleate (Span 85) and sodium stearate. In the same study [46], the authors tried to design myristic acid−in−water nanoemulsions but samples showed phase separation within few days after preparation. Delgado−Sanchez et al. [52] designed oil−in−oil−based emulsions using stearic acid (melting at ~ 68–71 °C) as phase change material, industrial ESQUIM FH−100 silicone oil as continuous phase and silicone−based non−ionic as surface−active agents. Sample stability was evaluated under several mechanical−thermal cycles and dispersed droplets proved to withstand more than 100 cycles in the calorimeter. More recently, Wang et al. [53] prepared stearic acid−based emulsions decorated with MAX phase powder (Ti_3AlC_2) and based on [BMIM]BF_4 ionic liquid. Samples proved good stability, excellent photo−thermal performance and enhanced storage capacity at temperatures around 65–70 °C. Cabaleiro et al. [38] presented the preparation and thermophysical profile of aqueous nanoemulsions loaded with 2–8 wt% contents of cetyl alcohol (melting temperature at ~ 48 °C). Considering a working temperature interval of 10 °C around solidification−melting phase changes, the 8 wt% emulsion exhibited an energy storage capacity up to 20 % superior to that of water.

Esters are organic materials that derive from the combination of a carboxylic acid and an alcohol by means of an esterification process. Like linear saturated fatty acids and primary alkanols, fatty acid methyl esters (FAMEs) also exhibit high fusion enthalpies, reduced subcooling degrees, low toxicity, and biodegradability. However, the functional group of FAMEs is methoxylated and therefore these materials are characterized by lower corrosivity and higher chemical stability than their corresponding precursors [54,55]. In addition, many fatty esters are commercially available in large amounts since they are industrially used for cosmetics, food, or textiles [56]. Although FAMEs are potentially interesting to produce phase change material emulsions, they have been limitedly tested. Fischer et al. [57] developed a rotor−stator approach to produce water−based slurries using a mixture of two commercial fatty acid esters (CrodaTherm™ 47 and CrodaTherm™ 53, at a mass ratio of 1:1) as phase change material and a mixture of two ethoxylated fatty alcohols (Brij™ S2 and Brij™ S100 at a mass ratio of 1:3) as emulsifier. According to differential scanning calorimetry (DSC) and T−history studies, the slurry loaded with 16 wt% of PCM doubled the apparent TES capacity of water in the temperature range of 47.5–50.0 °C. In a later work, Fischer et al. [58] completed the study evaluating the heat transfer performance of the 16 wt% emulsion in a test rig. Analyses showed Nusselt numbers up to 12–23 % larger for the PCM slurry in comparison to water under the same operation conditions. Materials such as methyl laureate or methyl myristate exhibit solid−liquid transitions within the temperature range usually accepted for thermal comfort in most countries [59,60] and have been categorized as potential PCMs for building applications such as cooling thermal management [61,62]. However, to the best of our knowledge, only methyl laureate was used as dispersed phase to produce aqueous (nano−) emulsions [63,64]. Moreover, in those articles [63,64] materials were envisaged for agricultural purposes such as pesticide delivery and not for energy−applications.

Present investigation explores the potential of methyl myristate to develop aqueous phase change material nanoemulsions as possible heat transfer and storage media. Nanoemulsion composition and formulation were optimized based on stability and calorimetric analyses in order to obtain colloidal suspensions with fine droplets, adequate fluidity and reduced subcooling. Solid−liquid phase change characteristics, rheological behavior, thermal conductivity and density were experimentally determined to analyze how temperature and/or dispersed content influence those thermal and physical properties. Finally, the thermal reliability and energy storage capacity of the optimized PCM nanoemulsions were also presented in order to assess the potential of developed slurries for thermal management at temperatures around 14 °C.

2. Materials and methods

2.1. Materials

Methyl myristate or methyl tetradecanoate, C_{14}Me, (onset melting temperature of T_m = 18 °C, mass purity of 99 %, Thermo Fisher Scientific, Kandel, Germany) was selected as phase change material, while *n*–hexadecane, C_{16}, (T_m = 18 °C, 99 %, Sigma Aldrich, Steinheim, Germany) and methyl stearate or methyl octadecanoate, C_{18}Me, (T_m = 41 °C, 96 %, Sigma Aldrich) were tested as nucleating agents/additives. A phosphate buffer solution, PBS, (40 mM and pH ~ 7.0) was prepared dissolving necessary amounts of monobasic and dibasic sodium phosphates (both with 99 % purity, Sigma Aldrich) in Milli−Q ultrapure water, W, produced with a resistivity of 18.2 MΩ·cm (Fisherbrand™ Accu20 System, Waltham, MA, USA). Non−ionic alkoxylated alcohol Brij™ S2 (98 %, HLB = 4.9, T_m = 42–46 °C, Sigma Aldrich) and anionic sodium dodecyl sulfate, SDS, (98 %, Sigma Aldrich) were used as surface−active agents. Sorbitane monooleate, Span 80, (HLB = 4.9) and polyoxyethylene sorbitan monooleate, Tween 80, (HLB = 15) were used during the preliminary experiments undertaken to optimize the formulation of the emulsifier system. *n*–hexane (98 %, Sigma Aldrich) served as solvent during the emulsification process. The information about the provenance and purity of reagents is summarized in Table S1 (Supporting materials).

2.2. Nanoemulsion formulation and preparation

O/W nanoemulsions were prepared by employing a dispersed phase mixture enriched in methyl myristate and following a solvent−assisted method derived from that originally described by Agresti et al. [65]. To obtain emulsions with fine droplets and good fluidity, dispersed phase content ranged from 2 to 12 % in mass, while emulsifier:dispersed phase and solvent:dispersed phase ratios were fixed at 1:8 and 5:1, respectively. Based on stability results (described in Section 3.1) and preliminary calorimetric analyses (Section 3.2), a SDS:Brij™ S2 mixture at an optimal mass ratio of 20:49 was selected as emulsifier while a C_{18}Me:C_{16}:C_{14}Me combination at a mass proportion of 1:3:36 was used as dispersed phase. In anionic SDS interfaces, H^+ and Na^+ ions are exchanged so that the counter−cation concentrations in the interfacial region are in large excess over the anion concentrations. As a result, interfacial H^+ concentrations in nanoemulsions are significantly different (1–2 orders of magnitude) from those in the bulk solution [66] and it can compromise the physical and chemical stability of the colloidal system. To avoid these variations, pH value was controlled and fixed to ~ 7.0 by employing a phosphate buffered solution 40 mM (99.4 wt% in water) as continuous phase.

First, two separated solutions were prepared: 1) the required amount of SDS was solubilized into the phosphate buffer and 2) the necessary amounts of Brij™ S2 and dispersed phase components (methyl myristate, *n*–hexadecane and methyl stearate) were solubilized in *n*–hexane (solvent). Once dissolved, the two solutions were joined in an Ultrasons–HD bath (J.P. Selecta S.A., Barcelona, Spain) and the mixture was sonicated (frequency: 40 kHz, power: 120 W, temperature: 50 °C) for 5 min. After, the pre−emulsion was further sonicated (frequency: 20 kHz, amplitude: 60 %, sonication mode: on−off pulse routine with a duty cycle of 50 %) for 20 min using a Bandelin Sonopuls HD 2200 ultrasound probe (Bandelin electronic GmbH, Berlin, Germany) together with a MS 72 titanium tip (2 mm in diameter). The preparation was then magnetically stirred for a minimum of 2 h at 90 °C to ensure complete *n*–hexane (solvent) evaporation. Finally, necessary amounts of milli−Q water were incorporated into the samples to obtain the predefined dispersed phase:emulsifier:continuos phase concentrations.

The hydrodynamic size distributions and ζeta potentials of suspended droplets were evaluated using a Zetasizer Nano ZS (Malvern Instruments Ltd., Worcestershire, UK) equipped with a 632.8 nm helium−neon laser [67]. Size determinations were performed according to

dynamic light scattering (DLS) principle, using 1−cm−path−length polystyrene cuvettes and a scattered angle of 173°. ζeta potential analyses were conducted based on electrophoretic light scattering (ELS) technique, utilizing DTS1070 folded capillary cells and a detection angle of 13°. Prior to ζeta potential determinations, nanoemulsions were diluted 10 times in the phosphate buffer solution (40 mM) and stirred at 400 rpm to ensure that registered signals were within the optimal sensitivity range. Reported results are based on a minimum of three parallel tests, each one averaging 15 runs of 10 s.

2.3. *Thermal−physical profile*

Phase−change temperatures (T_m for melting and T_c for crystallization) and latent heats (Δh_m for melting) were measured using a Q2000 differential scanning calorimeter, DSC, (TA Instruments, New Castle, USA) coupled with a RSC90 refrigerated cooling system. About 12 mg of sample was hermetically encapsulated in standard Tzero™ aluminum pans and the chamber was continuously flushed with nitrogen (purity > 99.999 %, flow rate: 50 cm^3/min). DSC cooling and heating thermograms were registered at scanning rates of β = 1–5 °C/min and temperatures ranging between 1 and 60 °C. The experimental uncertainties were estimated to be 0.3 °C (repeatability: 0.1 °C) and 1.2 J/g (repeatability: 0.7 J/g) for temperature and enthalpy determinations, respectively [68].

Apparent dynamic viscosities, μ, were obtained in the temperature range from 5 to 50 °C using a Physica MR−101 rotational rheometer (Anton Paar, Graz, Austria) working with a coaxial−cylinder geometry in a Couette flow field. The selected system consisted of a CC27/T200/SS cup (inner diameter: 28.9 mm) and a B−CC27/P6 bob (outer diameter: 26.7 mm, operating gap: 1.2 mm). The external cylinder was inserted into a C−PTD200 Peltier jacket to control sample temperature within 0.1 °C. Two different rheological tests were conducted. First, dynamic viscosity flow curves were measured at shear rates ramped up logarithmically from 1 to 100 s^{-1} with at least 5 measuring points per decimal. Then, temperature sweeps at a constant shear rate were performed in order to evaluate the variations of apparent viscosity during the phase change of dispersed droplets. Thus, dynamic viscosities were collected at a fixed shear rate of 10 s^{-1} while samples were heated from 5 to 50 °C at a constant heating rate of 0.1 °C/min. The declared uncertainty of dynamic viscosity determinations with this device and measuring system was lower than 4 % [38].

Thermal conductivities, λ, were investigated at temperatures from 4 to 50 °C by means of a THW−L2 device (Thermtest Inc., Hanwell, Canada) together with a dry bath also supplied by the same manufacturer [69]. The standard THW−L2 sensor was built on the principle of the transient short hot−wire method and consisted of an uninsulated alumel wire (diameter: ~0.1 mm and length: ~60 mm). The probe was placed vertically in a specifically−designed holder in which the sample completely surrounded the sensor, ensuring a free diffusion of the heat evolved by the device in all directions. An input time of 1 s and power supplies from 150 to 200 mW were selected to yield rises in sample temperature of ~ 2 °C. The experimental uncertainty of thermal conductivity determinations was estimated to be better than 5 %.

Densities, ρ, were studied in the temperature interval between 5 and 60 °C with a DMA 4500 oscillating U−tube densimeter (Anton Paar, Graz, Austria). The obtained values with this instrument showed a relative uncertainty of 0.05 % [70].

3. Results and discussion

3.1. *Optimization of nanoemulsion composition and stability*

In order to design stable nanoemulsions with fine droplets and adequate fluidity, the composition of the emulsifier mixture was optimized based on visual observations and dynamic light scattering (DLS) analyses.

First, the selection of the appropriate surfactant or mixture of surfactants for physically stabilizing the colloidal system requires the knowledge of their hydrophobic−lipophilic balance (HLB). The HLB value when a binary mixture of surfactants A and B was used (HLB_{blend}) can be calculated by means of the following equation, $HLB_{blend} = X{\cdot}HLB_A + (1–X){\cdot}HLB_B$, where X is the weight fraction of one of the surfactants (*e.g.* surfactant A) [71]. Here preliminary experiments were carried out by employing a series of emulsions prepared using the same mass proportions of methyl myristate as dispersed phase, phosphate buffer solution as continuous phase and an emulsifier binary mixture (composed of Span 80 and Tween 80 in different ratios). A required emulsifier HLB ~ 15 was found to be the optimal for the preparation of methyl myristate−based emulsions, in accordance with the results reported by Fischer et al. [57].

Then, various proportions of weighted amounts of different non−ionic and ionic surfactants (including several Tweens, Spans and Brijs combined or not with either SDS or dodecyltrimethylammonium bromide) with HLB_{blend} ~ 15 were tested in order to ensure an average hydrodynamic size of dispersed droplets < 200 nm and ζeta Potentials < –30 mV. These preliminary results showed that SDS:Brij™ S2 mixture at a mass ratio of 20:49 (HLB_{blend} = 15.1) was the most favorable emulsifier combination and it was chosen for the following experiments.

Once the composition of emulsifier mixture was optimized, methyl myristate−based emulsions containing 2–6 wt% of the dispersed phase were prepared. One day after the preparation, these emulsions exhibited average DLS diameters of ~ 320–430 nm at 25 °C and a phase separation within 3–4 weeks. However, the hydrodynamic size of emulsion droplets considerably reduced (up to below 200 nm) and stability improved (without visual phase separation within months) when one tenth of methyl myristate (C_{14}Me) was replaced by a mixture of *n*–hexadecane (C_{16}) and methyl stearate (C_{18}Me), tested also as nucleating agents. Based on DLS studies (see Table S2, Supporting material) and preliminary calorimetric tests (described in Section 3.2), a C_{18}Me:C_{16}:C_{14}Me mixture at a mass proportion of 1:3:36 was selected as dispersed phase to design all emulsions.

The day after preparation and at a temperature of 25 °C (dispersed droplets are in liquid phase), nanoemulsions formulated with 2–12 wt% contents of the optimized dispersed phase composition (C_{18}Me:C_{16}:C_{14}Me at a mass proportion of 1:3:36) exhibited mean droplet sizes in the range of ~ 140–190 nm and polydispersity indices lower than 0.3. The average diameters were slightly smaller (about ~ 5–10 nm inferior) when samples were investigated at the temperatures of 5–10 °C (dispersed particles are solid). As an example, Fig. 1a compares the size distributions obtained for the 12 wt% emulsions at different temperatures. Such differences could be attributed to the higher density of the dispersed phase material in solid state or to the effect of temperature on nanoemulsion physical stability. Thus, at high temperatures molecules move more energetically, and the harder and more frequent the collisions between droplets, the more likely they are to coalesce. However, deviations are within the 5 % of the declared uncertainty for this type of measurements. ζeta−potential measurements at 25 °C showed negative values in the range from−50 to−90 mV, which indicates that ionic−repulsion forces are strong enough to ensure good dispersion stability [72]. DLS results obtained at 25 °C for some representative samples are summarized in Table 1.

Given the thermodynamically−unstable nature of nanoemulsions, destabilization phenomena can arise when suspensions are stored in a reservoir or dispersed PCM particles undergo solid−liquid phase change. With the aim of detecting possible coalescence or phase separation issues in those two situations, the hydrodynamic size of formulated emulsion droplets was monitored for samples: *i)* maintained static for over a month and *ii)* subjected to 30 heating−cooling cycles at temperatures ranging between 5 and 50 °C. In both cases DLS measurements were conducted at 25 °C (dispersed droplets are liquid). As presented in Fig. 1b, when stored under static conditions, suspensions showed moderate increases in the average diameter of dispersed

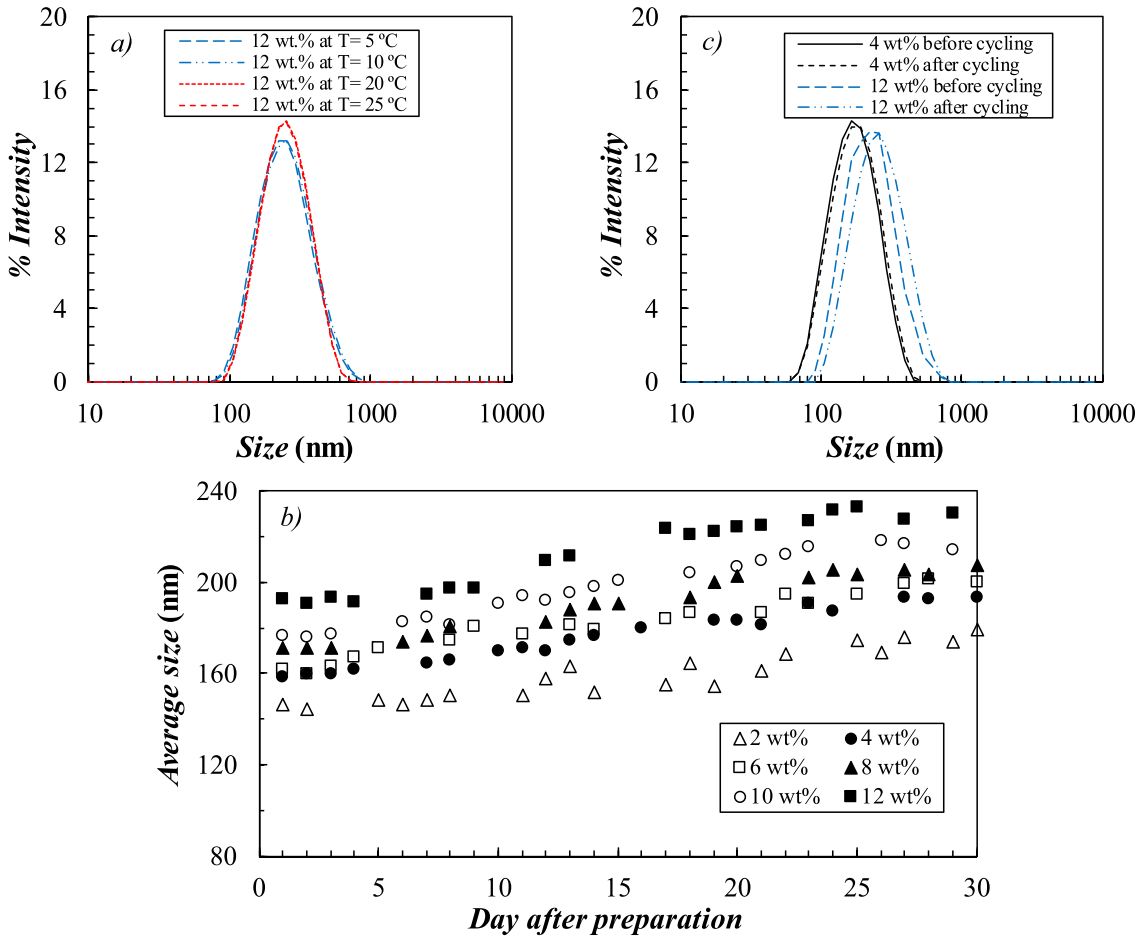

Fig. 1. (a) Temperature, (b) temporal and (c) freeze–thaw stability assessments based on dynamic light scattering measurements for O/W nanoemulsions composed of a dispersed phase mixture (2–12 wt%) enriched in methyl myristate. Results obtained at $T = 25$ °C unless otherwise indicated.

Table 1
ζ–potential, hydrodynamic DLS size and polydispersity index (PDI) measurements of optimized C_{18}Me:C_{16}:C_{14}Me–in–water nanoemulsions. Results obtained at 25 °C.

Final nanoemulsion composition				**1st day**		**30th day**
Dispersed phase (C_{14}Me)	(C_{16})	(C_{18}Me)	Surfactant (SDS:Brij™ S2 at 20:49 w/w)	Zeta potential	Size (PDI)	Size (PDI)
1.80 wt %	0.15 wt%	0.05 wt %	0.25 wt%	−56 mV	146 nm (0.16)	179 nm (0.29)
3.60 wt %	0.30 wt%	0.10 wt %	0.50 wt%	−60 mV	158 nm (0.28)	193 nm (0.28)
5.40 wt %	0.45 wt%	0.15 wt %	0.75 wt%	−66 mV	162 nm (0.16)	200 nm (0.27)
7.20 wt %	0.60 wt%	0.20 wt %	1.00 wt%	−72 mV	171 nm (0.24)	207 nm (0.27)
9.00 wt %	0.75 wt%	0.25 wt %	1.20 wt%	−81 mV	176 nm (0.24)	214 nm (0.25)
10.80 wt%	0.90 wt%	0.30 wt %	1.50 wt%	−87 mV	192 nm (0.28)	230 nm (0.23)

particles (less than ~ 40 nm) over the timeframe of study. In addition, no significant change in the size distribution of emulsified droplets was detected when samples were subject to 30 thermal cycles, except in the case of 12 wt% concentration, in which the average particle size increased by ~ 50 nm (Fig. 1c).

3.2. Crystallization and melting phase change characteristics

The temperatures and enthalpies of solid–liquid transitions were investigated by differential scanning calorimetry (DSC). The cooling and heating thermograms of methyl myristate (C_{14}Me) in bulk form are shown in Fig. 2a and b. A single endothermic peak with an onset temperature at $T_m = 18.4$ °C and associated latent heat of $\Delta h_m = 205.4$ J/g was observed in the heating process of bulk–C_{14}Me. These values agree quite well with previous melting data reported for this material in the literature [73–75]. As for the cooling DSC scans, two close and almost over–imposed peaks were registered with an onset temperature at 16.7 °C.

When we used only methyl myristate as dispersed phase to produce the emulsions, samples exhibited sub–cooling degrees of about 12–13 °C (a representative 6 wt% C_{14}Me–in–water emulsion is presented in Fig. S1, Supporting materials). Besides, when cooled down to 1 °C (lower temperatures were avoided to prevent a possible freezing of continuous phase), only a small portion of the dispersed material had completely undergone liquid–solid phase change. With the aim of reducing the subcooling of emulsified droplets, the composition of the dispersed phase was optimized. Preliminary calorimetric tests were performed for samples loaded with 6 wt% contents of three

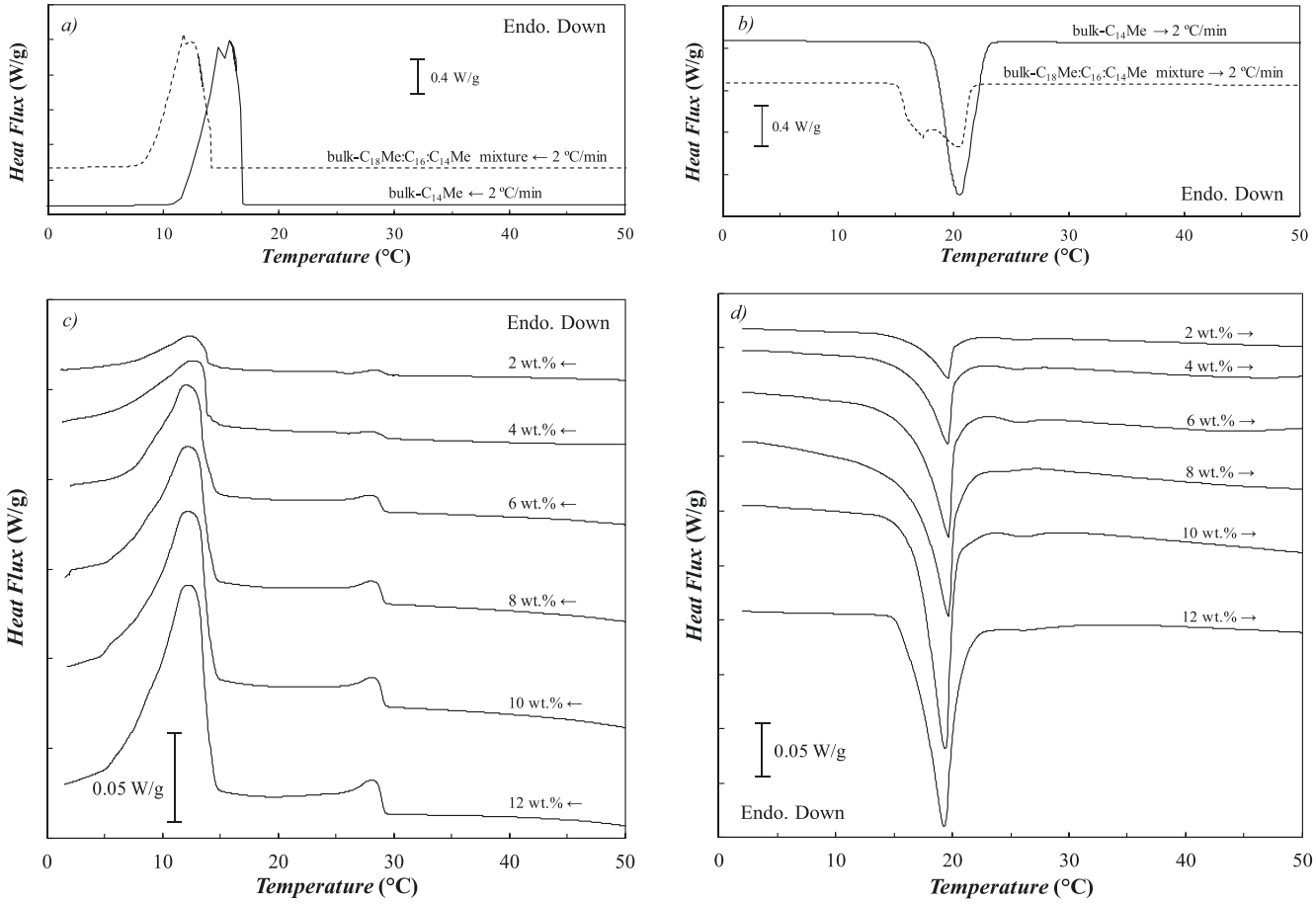

Fig. 2. (a,c) Cooling and (b,d) heating DSC thermograms obtained at $\beta = 2$ °C/min for (a,b) bulk−C_{14}Me and bulk−C_{18}Me:C_{16}:C_{14}Me materials and (c,d) optimized C_{18}Me:C_{16}:C_{14}Me−in−water nanoemulsions.

three−component mixtures of methyl myristate:*n*–hexadecane:methyl stearate (at C_{18}Me:C_{16}:C_{14}Me proportions of 2:2:36, 1:3:36 and 0:4:36) selected based on DLS stability analyses (Table S2, Supporting materials). Among the investigated samples, only emulsified droplets prepared using C_{18}Me:C_{16}:C_{14}Me proportions of 2:2:36 and 1:3:36 meaningfully underwent the solid−liquid when cooling down to 1 °C (Fig. S1, Supporting materials). Trying to reach a compromise between the smaller droplet size and a lower degree of subcooling, the C_{18}Me:C_{16}:C_{14}Me mixture at a mass proportion of 1:3:36 was considered to be the most convenient for preparing the PCM nanoemulsions.

The DSC cooling and heating curves for the the optimized:methyl stearate:*n*–hexadecane:methyl myristate mixture (at a C_{18}Me:C_{16}:C_{14}Me mass proportion of 1:3:36, selected as described in the previous paragraph) in bulk form are also presented in Fig. 2a and 2b. Two over−imposed endothermic events (with peak temperatures at 17.2 and 20.6 °C and a total enthalpy of $\Delta h_m = 193.3$ J/g) are registered in the heating curve of bulk−C_{18}Me:C_{16}:C_{14}Me mixture. Complex phase change behaviors were previously reported for mixtures of *n*–alkane and saturated methyl/ethyl esters [50,73,76,77]. Thus, depending on the length of alkyl chains, parity or composition, the formation of co−crystals, eutectic or solid−solutions is quite common in their solid−liquid phase diagrams. However, to the best of our knowledge, the solid−liquid phase equilibria of C_{18}Me:C_{16}:C_{14}Me ternary system was not investigated in the literature. Two close peaks are observed in the cooling thermogram with an onset temperature at 14.5 °C. Like bulk−C_{14}Me, bulk−C_{18}Me:C_{16}:C_{14}Me exhibits a moderate subcooling degree (lower than ~ 2 °C).

Fig. 2c and d show the cooling and heating DSC thermograms measured for nanoemulsions formulated using 2–12 wt% contents of that optimized C_{18}Me:C_{16}:C_{14}Me combination. Determined phase change temperatures and enthalpies are summarized in Table 2. The heating curves of the PCM suspensions (see Fig. 2d) do not show the same double peak behavior observed for the bulk−C_{18}Me:C_{16}:C_{14}Me mixture. Instead, in the case of the emulsified C_{18}Me:C_{16}:C_{14}Me

Table 2
Phase change characteristics of optimized C_{18}Me:C_{16}:C_{14}Me−in−water nanoemulsions obtained at $\beta = 2$ °C/min.

Sample composition (final wt%)		Cooling	Heating		
Dispersed phase (C_{18}Me:C_{16}:C_{14}Me at 1:3:36 w/w/w)	***Surfactant*** (SDS:Brij™ S2 at 20:49 w/w)	***T*** (°C)	T_m (°C)	Δh_m (kJ/kg) (experimental)	(estimated according to Eq.(1))
2.00 wt%	0.25 wt%	28.4[p] 13.7	16.8	2.87	3.47
4.00 wt%	0.50 wt%	28.0[p] 13.9	16.8	5.60	6.95
6.00 wt%	0.75 wt%	28.1[p] 13.8	16.7	8.52	10.43
8.00 wt%	1.00 wt%	28.3[p] 13.9	16.8	10.8	13.91
10.00 wt%	1.25 wt%	28.3[p] 14.0	16.8	13.7	17.39
12.00 wt%	1.50 wt%	28.5[p] 14.1	16.6	16.6	20.87

[p] Peak temperatures.

droplets, there is a major peak with onset temperatures at ~ 16–17 °C (close in value to the result obtained for that material in bulk form) and a secondary peak at ~ 26 °C. This secondary endothermic event, more appreciable with rising concentration of dispersed phase, may be due to the presence of a higher content of methyl stearate (T_m = 41 °C) in certain droplets. Two exothermic processes are registered in the cooling scans of PCM nanoemulsions. The smaller one (with a peak temperature of ~ 28 °C) may also be due to the existence of some PCM droplets with a higher proportion of C_{18}Me. The larger peak (due to crystallization of dispersed C_{18}Me:C_{16}:C_{14}Me droplets) has an onset temperature ~ 14 °C, similar to that bulk−C_{18}Me:C_{16}:C_{14}Me mixture. Thus, even if solid−phase transitions of optimized C_{18}Me:C_{16}:C_{14}Me−droplets extended in a wider temperature than investigated bulk−materials, formulated phase change materials also exhibit moderate subcooling degrees ($\Delta T_{subcooling}$ ~ 3 °C).

Latent heats increase with the rising content of dispersed phase with an almost linear dependence. Nevertheless, these values are 18–23 % lower than predicted using the following mass relation:

$$\Delta h_{m,PCME} = \varphi_{droplets} \cdot \Delta h_{m,\ droplets} \quad (1)$$

where Δh_m is the melting latent heat, φ is the mass fraction while PCME subscript stands for phase change material nanoemulsion. Lower enthalpies of fusion than predicted by Eq. (1) have been reported for PCM−in−water nanoemulsions [26,38,65]. Such reductions have been attributed in the literature [30,65] to the fact that part of the material confined in the nanodroplets may be taking part of the surface layer, which can considerably affect its crystallinity (when compared to the bulk form of that same material).

Since the main advantage of PCMEs is their superior heat storage capabilities, it is essential to verify that the solid–liquid temperatures or latent heats of emulsified PCM droplets do not significantly change throughout storage or after thermal cycling. In this investigation two different analyses were conducted with the aim of assessing the storage/cycling reliability of developed nanoemulsions. As an example, Fig. 3 shows the results of these two tests for the nanoemulsion loaded with 12 wt% of the optimized C_{18}Me:C_{16}:C_{14}Me mixture. First, one day after their preparation, samples were subject to 100 cooling–heating cycles at a scanning rate of β = 10 °C/min in the temperature range from 2 to 60 °C. No differences were appreciated among the scans of the different performed cycles (Fig. 3a). Eight months after their preparation, 12 wt% dispersion was also subject to 500 cooling–heating cycles (Fig. 3b). When comparing the two analyses, the cooling peak is slightly narrower in the case of the 8 month–stored sample, even if the onset temperatures (T_c = 14.3 °C and T_m = 16.7 °C) and melting latent heat are similar to those reported in Table 2. No significant changes were appreciated among the different runs of this second cycling test.

3.3. Heat storage capacity

The total heat capacity of developed nanoemulsions can be determined by integrating the DSC heat flux signals in the desired temperature range [78]. Fig. 4a compares the enthalpy versus temperature curves obtained for 6 wt% and 12 wt% optimized C_{18}Me:C_{16}:C_{14}Me−in−water nanoemulsions from experimental calorimetric analyses and the data calculated for water from NIST Database [79] (a temperature of T = 2 °C was considered as reference point in all cases). As it can be observed, the total heat capacity of formulated nanoemulsions is larger than that of the water in the considered temperature range. Nevertheless, those enhancements strongly rely on the temperature range covered by the phase change material nanoemulsion (ΔT) according to the following equation:

$$\Delta h_{total} = \varphi_{droplets} \cdot \Delta h_{m,\ droplets} + \Big((\varphi_{droplets} + \varphi_{surfactant}) \cdot c_{p,C14Me} + (1 - \varphi_{droplets} - \varphi_{surfactant}) \cdot c_{p,water} \Big) \cdot \Delta T \quad (2)$$

where Δh_{total} is the total heat capacity, Δh_m is the melting latent heat, φ is the mass fraction and c_p is the isobaric heat capacity. As done by Huang et al. [78], given the minor contributions of nucleating agents and surfactants to the total TES capacity, their isobaric heat capacities were considered to be the same as that of the main component of the dispersed phase (methyl myristate, C_{14}Me, [80] in our study). As shown in Fig. 4b, the improvement in the stored energy strongly reduces as the working temperature interval enlarges. Thus, in the case of the 12 wt% sample, enhancements in Δh_{total} decrease from 31 % to 18 % as ΔT increases from 10 to 15 °C.

3.4. Rheological behavior and apparent dynamic viscosity

The apparent viscosity, μ, of the working fluid has a direct impact on the drop pressure and pumping power consumption of the thermal facility. Hence, Newtonian low−viscosities are preferable, particularly in those systems in which fluids must flow long distances or at high shear rates. Fig. 5 depicts the shear viscosity−shear rate response of optimized C_{18}Me:C_{16}:C_{14}Me−in−water nanoemulsions at two representative temperatures: 5 °C (droplets in solid phase) and 30 °C (liquid droplets). Flow curves of milli−Q water and the phosphate buffer solution (PBS, 40 mM) are also presented for comparison. Viscosities obtained for water showed maximum deviations of 3.6 % with previous literature [79]. The results measured for the PBS used as continuous phase are slightly higher (less than 3 %) than water. In addition, values of μ = 3.57 mPa·s (1.7 % higher than the data reported in [81]) and μ = 3.81 mPa·s were determined at 30 °C for bulk−methyl myristate and the bulk−C_{18}Me:C_{16}:C_{14}Me mixture (at the optimized 1:3:36 mass proportion), respectively.

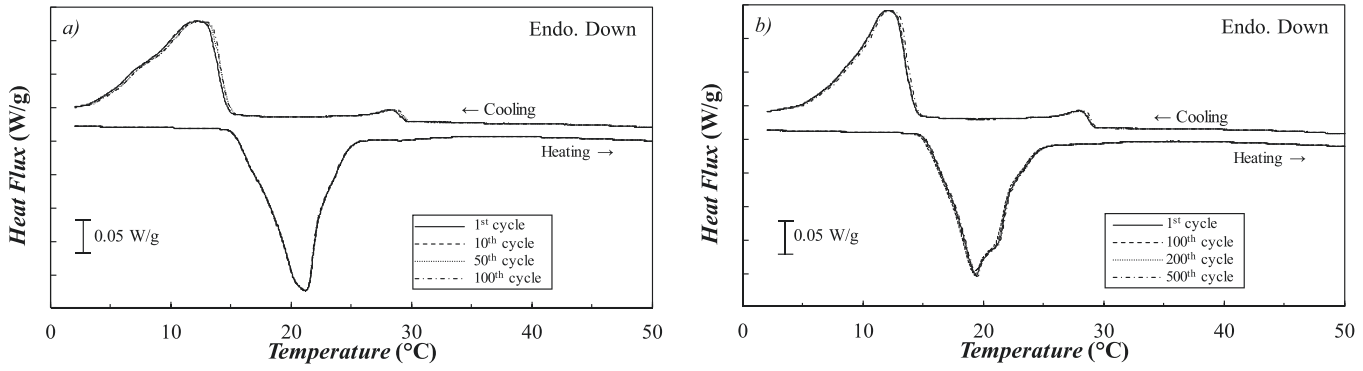

Fig. 3. Cooling−heating cycling tests for the aqueous nanoemulsion loaded with 12 wt% of the optimized C_{18}Me:C_{16}:C_{14}Me dispersed phase (a) one day after the preparation and (b) 8 months after preparation. DSC curves obtained at β = 10 °C/min from different runs are mainly superimposed.

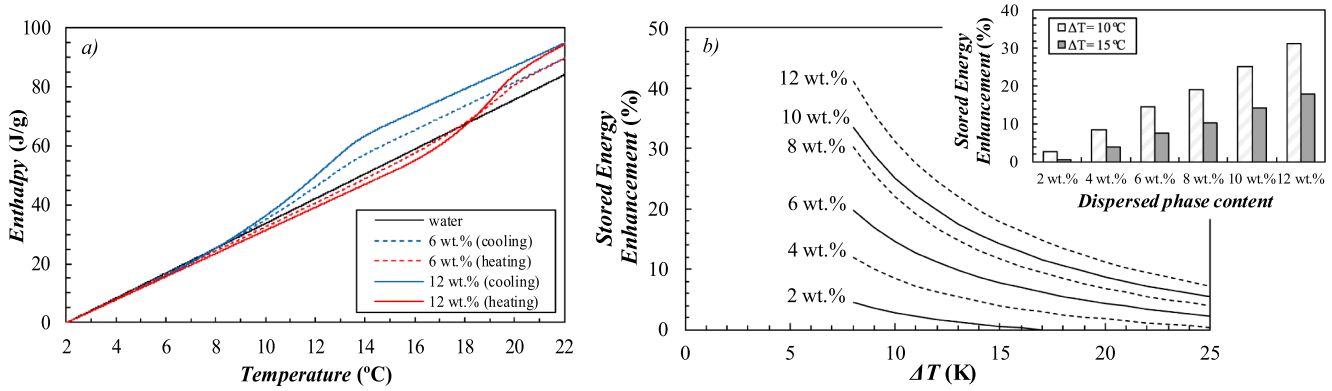

Fig. 4. (a) Enthalpy versus temperature curves, taking $T = 2$ °C as reference temperature, and (b) enhancements in thermal energy storage capacity as a function of the temperature interval covered by the thermal fluid, ΔT, for some representative C_{18}Me:C_{16}:C_{14}Me−in−water nanoemulsions. Readers are suggested to refer the electronic version of the article for colors.

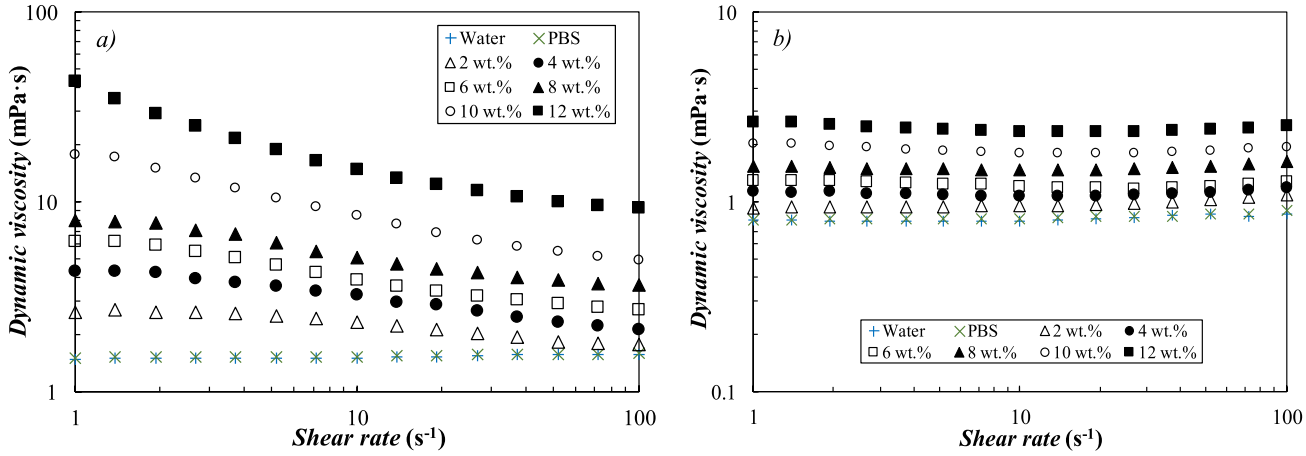

Fig. 5. Shear rate−shear viscosity flow curves obtained for water, the phosphate buffer solution (PBS) and the optimized C_{18}Me:C_{16}:C_{14}Me−in−water nanoemulsions prepared with different percentages of dispersed phase (2–12 wt%) at (a) 5 °C and (b) 30 °C.

Overall, unlike water and PBS (40 mM), the optimized nanoemulsions exhibit a non−Newtonian shear−thinning (pseudoplastic) behavior at 5 °C (emulsified droplets are solid), which is more noticeable with rising content of dispersed phase (see Fig. 5a). Instead, as can be appreciated in Fig. 5b, samples are mainly Newtonian at 30 °C (liquid droplets). Similar changes from shear−thinning to Newtonian behavior when dispersed droplets undergo solid−liquid transition were also observed for other PCM−in−water nanoemulsions [52,82]. As expected, apparent dynamic viscosity strongly increases with rising content of dispersed phase. At 100 s^{-1}, relative viscosities (calculated as the ratio between the viscosity of the corresponding nanoemulsion and that of the PBS used as continuous phase, *i.e.* μ_{PCME}/μ_{PBS}) reached 6.2 (at 5 °C) and ~ 2.9–3.0 (30–50 °C) for the sample loaded with 12 wt% of the optimized C_{18}Me:C_{16}:C_{14}Me mixture. These changes in (non) −Newtonian flow curves and relative viscosity depending on the solid/liquid physical state of dispersed phase were attributed to the fact that particle−particle interactions responsible for higher viscosities and shear−thinning behaviors lessen as the suspended PCM droplets melt [83]. Even so, it must also be pointed out that, in addition to the physical state and concentration of dispersed particles, the viscosity of this type of colloids also strongly relies on design parameters such as the size/shape of dispersed droplets or the emulsifying system. In fact, the concentration and surfactant type influence the micelle structure created by the surfactant interface as well as the nature of the repulsive forces among PCM particles (stearic/ionic stabilization), which in turn have also a direct impact on sample viscosity [23]. As an example, Zhang et al. [84] observed that the viscosity of the formulated systems could considerably change by just changing the used surfactant.

Since PCM slurries are typically operated at temperatures near the phase change transition, further understanding the flow behavior in this

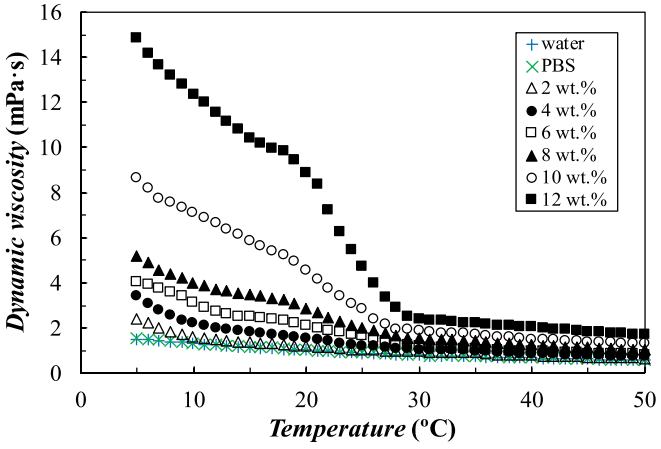

Fig. 6. Apparent viscosity−temperature curves obtained at a constant shear rate of $\dot{\gamma} = 10\ s^{-1}$ while heating at $\beta = 0.1$ °C/min for bulk water, the phosphate buffer solution (PBS) and optimized C_{18}Me:C_{16}:C_{14}Me−in−water nanoemulsions prepared with different percentages of dispersed phase (2–12 wt%).

region (also known as mushy zone) is also important for their practical application [83]. Hence, temperature ramp tests at a constant shear rate ($\dot{\gamma}$ = 10 s^{-1}) were also conducted to evaluate modifications in the apparent viscosity of PCM nanoemulsions during the melting transition of dispersed droplets. Fig. 6 shows the viscosity−temperature curves obtained for water, the PBS (40 mM) and the six optimized C_{18}Me:C_{16}:C_{14}Me−in−water nanoemulsions while heating from 5 to 50 °C at β = 0.1 °C/min. Outside the phase change region, prepared PCM nanoemulsions follow the universal fluid behavior of liquids and therefore dynamic viscosity decreases with rising temperature. However, an abrupt viscosity drop, more remarkable with the increasing content of dispersed phase, is observed in this property in the temperature range from 15 to 30 °C in which emulsified droplets are expected to melt. Similar perturbations in viscosity−temperature curves were reported in the literature for other phase change materials slurries [18,21,25,85]. As reviewed in [23,32], authors have attributed these "perturbations" to shape/volume modifications of suspended PCM particles. Thus, the dispersed material is expected to expand while undergoing melting transition. In addition, as already discussed, colloidal suspensions of liquid droplets usually exhibit lower apparent viscosity ratios than suspensions of solid particles with comparable particles sizes and continuous phase. Other plausible elucidations for such a behavior may be: *i)* a possible tank−tread−like motion inside suspended liquid droplets, *ii)* the better ability of liquid droplets to deform when sheared *iii)* modifications in the elastic or non−elastic nature of particle collisions depending on the solid/liquid physical state of dispersed phase [21,85].

3.5. Thermal conductivity

As illustrated in Fig. 7a, the temperature dependence of thermal conductivity, λ, was experimentally analyzed in the range between 4 and 50 °C for milli−Q water, the phosphate buffer solution (PBS, 40 mM) and the optimized C_{18}Me:C_{16}:C_{14}Me−in−water nanoemulsions. Results obtained for water showed a maximum deviation of 2.9 % with well−stablished values reported in the literature [79]. At investigated temperature conditions, the thermal conductivities determined for the PBS mixture used as continuous phase were slightly inferior to those of water (with a maximum difference of 0.5 %). Much lower λ values, ~0.15 W/(m·°C), were measured in liquid phase (30 °C) for both bulk−methyl myristate (C_{14}Me) and the bulk−C_{18}Me:C_{16}:C_{14}Me mixture (at 1:3:36 ratio). In the case of methyl myristate, this result is close to the data reported by Zheng et al. [86] and Fan et al. [87]. Given the lower λ value of bulk−C_{18}Me:C_{16}:C_{14}Me in comparison to water, the thermal conductivity of developed PCM nanoemulsions decreased with rising content of dispersed phase. Obtained reductions in this property are larger at temperatures when suspended droplets are melted (up to ~ 17 % lower than water for the 12 wt% nanoemulsion) than when they are in solid phase (~ 9% inferior to water for that same concentration). These results agree with the fact that most organic materials such as fatty acid esters exhibit lower thermal conductivities when they are liquid than when they are solid (usually, in the range from 0.30−0.35 W/(m·°C) [88]).

Owing to the importance of thermal conductivity for several heat transfer applications, considerable research effort has been devoted to develop suitable models to predict the variations in this property for two−phase materials. In addition to the type and morphology of the dispersed/embedded material, the effective thermal conductivity of such multiphase systems varies significantly from well−dispersed configurations to dispersions with interconnected networks, particle clustering or aggregation. Maxwell [89] proposed the first semi−empirical relationship to calculate the thermal conductivity of low−concentrated

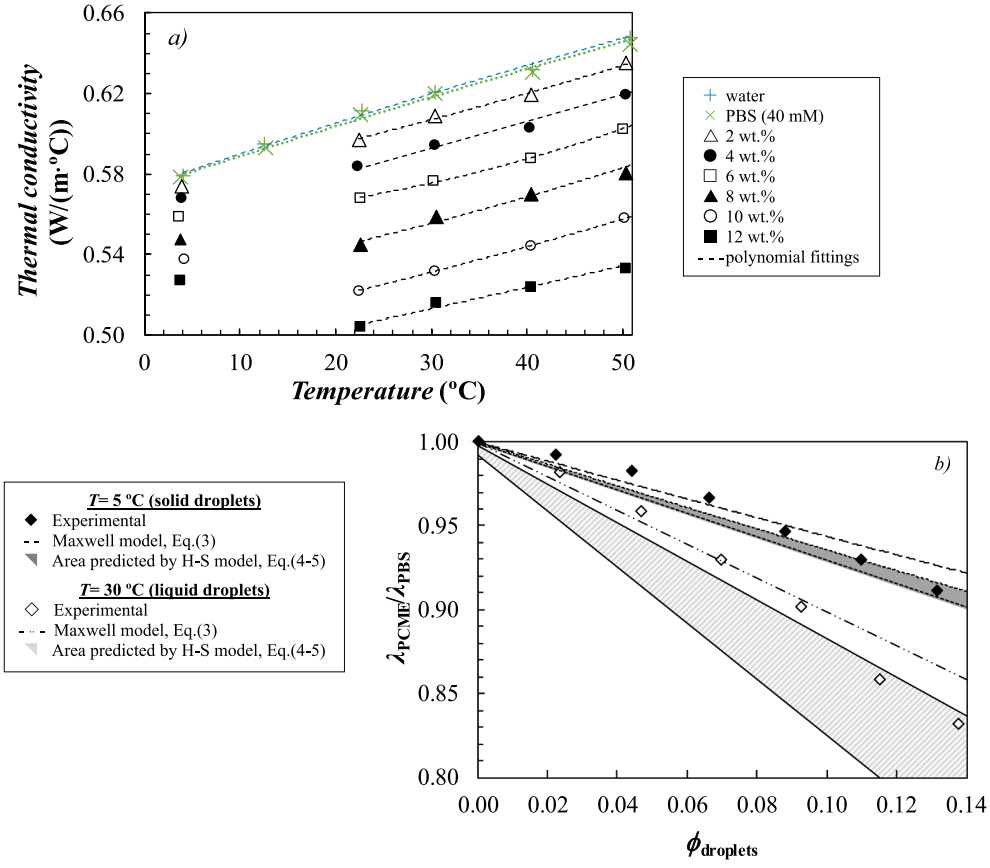

Fig. 7. (a) Temperature dependence of thermal conductivity and (b) relative thermal conductivity (defined here as $\lambda_{PCME}/\lambda_{PBS}$ ratio) as a function of volume fraction, $\phi_{droplets}$.

dispersions of non−interacting spheres:

$$\lambda_{PCME}/\lambda_{PBS} = \frac{2\cdot\lambda_{PBS} + \lambda_{droplets} + 2\cdot\phi_{droplets}\cdot(\lambda_{droplets} - \lambda_{PBS})}{2\cdot\lambda_{PBS} + \lambda_{droplets} - \phi_{droplets}\cdot(\lambda_{droplets} - \lambda_{PBS})} \quad (3)$$

where λ is the thermal conductivity, ϕ is the volume fraction while PCME and PBS subscripts stand for phase change material nanoemulsion and phosphate buffer solution, respectively. Using a variational approach based on classical effective−medium theory, Hashin−Shtrikman (H−S) [90] derived the following lower and upper bounds of effective thermal conductivity:

$$\lambda_{PCME}/\lambda_{PBS} = 1 + \frac{2\cdot\phi_{droplets}\cdot(\lambda_{droplets}/\lambda_{PBS} - 1)}{1 + \lambda_{droplets}/\lambda_{PBS} - \phi_{droplets}\cdot(\lambda_{droplets}/\lambda_{PBS} - 1)} \quad (4)$$

$$\lambda_{PCME}/\lambda_{PBS} = \lambda_{droplets}/\lambda_{PBS}\cdot\left(1 - \frac{2\cdot(1-\phi_{droplets})\cdot(\lambda_{droplets}/\lambda_{PBS} - 1)}{2\cdot\lambda_{droplets}/\lambda_{PBS} - \phi_{droplets}\cdot(\lambda_{droplets}/\lambda_{PBS} - 1)}\right) \quad (5)$$

Fig. 7b presents the dependence of $\lambda_{PCME}/\lambda_{PBS}$ on the volume fraction of dispersed droplets at 5 and 30 °C. As shown in that figure, there is a considerably good agreement between experimental results and values predicted using either Maxwell equation [89] or the lower bound of H−S model [90], particularly when suspended droplets are solid. Thus, at 5 °C (when droplets are in solid phase), maximum deviations between experimental and calculated values are 1.0 % by using Eq. (4) and 1.8 % with Eq. (3). At temperatures between 30 and 50 °C (droplets are liquid), maximum deviations reach 2.0 % by using Eq. (4) and 4.6 % with Eq. (3). The goodness of Maxwell [89] to predict the experimental thermal conductivities of other PCM nanoemulsions was also reported in the literature by Morimoto et al. [24,91] or Saarinen et al. [92], as examples.

3.6. Density and thermal expansivity

Density, ρ, was experimentally determined for water, the phosphate buffer solution (PBS, 40 mM) and the optimized C_{18}Me:C_{16}:C_{14}Me nanoemulsions. Values of 860.3 and 859.1 kg/m^3 were also measured in liquid phase (30 °C) for bulk−methyl myristate and bulk−C_{18}Me:C_{16}:C_{14}Me, respectively. The density of methyl myristate deviates less than 0.07 % compared to the value reported by Pratas et al. [93]. Fig. 8a depicts the temperature evolution of this property in the interval between 5 and 50 °C. Densities obtained for the phosphate buffer solution were slightly higher (~ 2 kg/m^3) than those of water. Nanoemulsion ρ values decreased with the rising content of dispersed phase, particularly when emulsified droplets are melted. Thus, when compared to water, reductions in this property at the higher content of C_{18}Me:C_{16}:C_{14}Me (12 wt%) reached 1.9 % at 5–7 °C and 2.6 % at 60 °C. The influence of dispersed phase concentration of multiphase systems can be predicted by means of the following weight−averaged equation [94]:

$$\frac{1}{\rho_{PCME}} = \frac{\varphi_{droplets}}{\rho_{droplets}} + \frac{\varphi_{SFT}}{\rho_{SFT}} + \frac{1 - \varphi_{droplets} - \varphi_{SFT}}{\rho_{PBS}} \quad (6)$$

where ρ is the density, φ is the mass fraction, while PCME, SFT and PBS subscripts stand for phase change material nanoemulsion, surfactant and phosphate buffer solution, respectively. In the studied system, experimental results deviated from the values calculated according to Eq. (6) up to 0.86 % at 5–7 °C (when dispersed particles are solid) and up to 0.66 % at 25–60 °C (liquid droplets).

In the case of PCM nanoemulsions, accurate density values are not only necessary to assess the volumetric storage density of the material, but also to quantify the volumetric changes experienced by the slurries with particle phase change and temperature. Density modifications in the temperature interval from 7 to 25 °C (in which C_{18}Me:C_{16}:C_{14}Me droplets are expected to melt) increased with rising content of dispersed phase from 0.42 % for water to 0.77 % for the 12 wt% nanoemulsion. Isobaric thermal expansivity, α_p, can also be obtained from numerical differentiation of experimental density data with respect to temperature using the following expression:

$$\alpha_p = -(1/\rho)\cdot(\partial\rho/\partial T)_{p=0.1MPa} \quad (7)$$

In order to calculate α_p values, experimental density−temperature curves in the interval from 25 to 60 °C (emulsified droplets are in liquid phase) were first fitted using two second−order polynomials, *i.e.* $\rho = a_2\cdot T^2 + a_1\cdot T + a_0$, with a_i being the fitting parameters. The isobaric thermal expansivities of water, the buffer solution and some representative optimized C_{18}Me:C_{16}:C_{14}Me nanoemulsions are shown in Fig. 8b. As can be observed, when comparing with PBS, this property increases with both rising temperature and content of dispersed phase. This behavior may be attributed to the higher thermal expansivity of the emulsified droplets/particles. Thus, that methyl myristate, main component of the dispersed phase, exhibits $\alpha_p \sim 9\cdot10^{-4}$ K^{-1} [93].

4. Conclusions

Stable PCM nanoemulsions were produced by dispersing 2–12 % contents of a methyl stearate:*n*–hexadecane:methyl myristate mixture (at a mass proportion of 1:3:36) in water with the assistance of SDS and Brij^{TM} S2 surfactants (mass ratio of 20:49). After preparation, optimized nanoemulsions exhibited dispersed droplets with strong repulsive

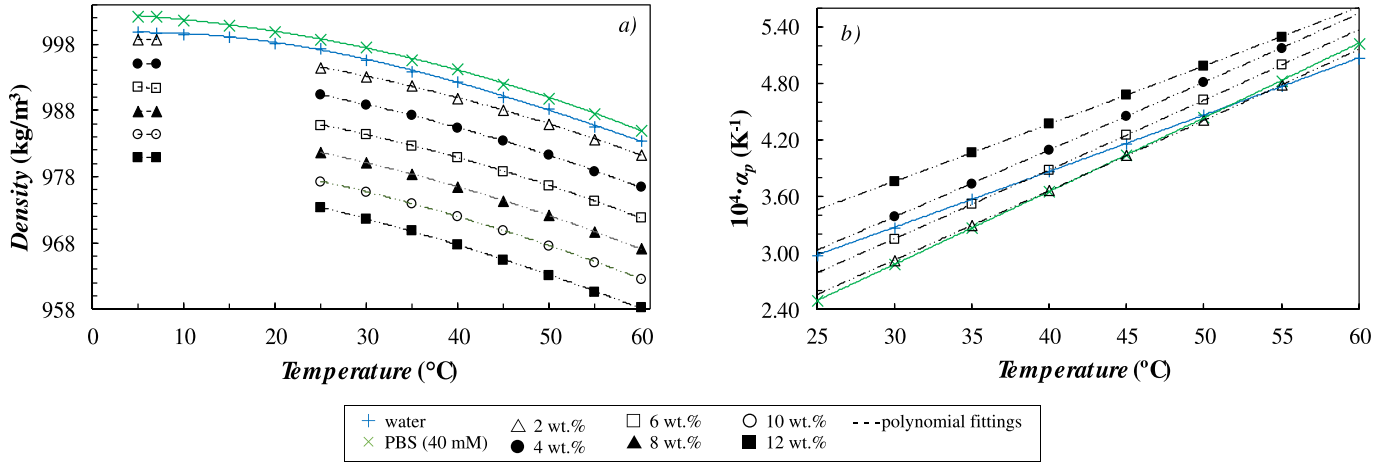

Fig. 8. (a) Density and (b) isobaric thermal expansivity, α_p, as a function of temperature for water, the phosphate buffer solution (PBS) and the optimized C_{18}Me:C_{16}:C_{14}Me−in−water nanoemulsions prepared with different percentages of dispersed phase (2–12 wt%).

electrostatic charges (ζeta−potentials stronger than−50 mV) and average sizes in the range of ∼ 140–190 nm. Stability analyses throughout storage time or after thermal cycling only showed moderate increases in droplet size. Calorimetric investigations proved the potential of selected PCM mixture to produce phase change material slurries with reduced subcooling (∼ 3 °C). Even if the addition of *n*–hexadecane did not have a significant influence on reducing the subcooling degree of dispersed phase, the presence of *n*–alkane was proven effective in reducing droplet size and improving sample physical stability. At low temperatures when suspended droplets were solid, nanoemulsions presented a shear thinning behavior, more noticeable with rising dispersed phase content. However, samples showed desirable Newtonian viscosities above the melting temperature of dispersed droplets. The thermal conductivities of optimized nanoemulsions were 51–250 % larger in comparison to bulk−PCM mixture, but up to 17 % lower when contrasted with water. According to volumetric studies, the density of PCM slurries modified by ∼ 0.8 % (almost doubling the density variations of water) in the temperature range from 7 to 25 °C, in which emulsified droplets undergo solid–liquid transition. Thermal reliability tests based on differential scanning calorimetry demonstrated that the solid−liquid phase transitions of emulsified droplets did not considerably change after samples were stored for 8 months and subject to 500 cooling–heating processes. Finally, optimized dispersions proved larger thermal energy storage capacity than water. Therefore, the sample loaded with 12 wt% of emulsified droplets presented enhancements of 31 % and 18 % when considering operating temperature intervals (around the melting−crystallization of optimized dispersed phase) of 10 and 15 °C, respectively. Further analyses of heat transfer performance and pumping power consumption are suggested to explore the implementation of developed PCMEs in practical applications.

CRediT authorship contribution statement

D. Cabaleiro: Conceptualization, Formal analysis, Investigation, Methodology, Writing – original draft. **C. Hermida−Merino:** Formal analysis, Investigation, Methodology, Writing – original draft. **S. Losada−Barreiro:** Investigation, Resources, Writing – review & editing. **F. Agresti:** Formal analysis, Methodology, Writing – review & editing. **L. Lugo:** Resources, Writing – review & editing, Formal analysis. **D. Hermida−Merino:** Formal analysis, Validation, Writing – review & editing. **M.M. Piñeiro:** Project administration, Resources, Supervision, Writing – review & editing.

Declaration of competing interest

The authors declare the following financial interests/personal relationships which may be considered as potential competing interests: Filippo Agresti reports financial support was provided by Consiglio Nazionale delle Ricerche. Luis Lugo reports financial support was provided by Spanish Ministry of Science Technology and Innovations and ERDF A way of making Europe. Sonia Losada reports financial support was provided by Spanish Ministry of Science Technology and Innovations and ERDF A way of making Europe. David Cabaleiro reports financial support was provided by Spanish Ministry of Science Technology and the European Union NextGenerationEU PRTR. Daniel Hermida-Merino reports was provided by Spanish Ministry of Science Technology and the European Union NextGenerationEU PRTR.

Data availability

Data will be made available on request.

Acknowledgements

Project “PCM Cool” financed by CNR Italy. Grant PID2020-112846RB-C21 funded by MCIN/AEI/10.13039/501100011033 as well as Grant PID2022-136443OB-I00 funded by MCIN/AEI/ 10.13039/501100011033 and by “ERDF A way of making Europe”. D. Cabaleiro is a recipient of a “Juan de la Cierva” contract (agreement IJC2020-043779-I) supported by the Spanish “Ministerio de Ciencia e Innovación” and the European Union NextGenerationEU/PRTR. D. Hermida-Merino acknowledges a “Maria Zambrano” contract for the University of Vigo, financed by the Spanish “Ministerio de Ciencia e Innovación” and the European Union NextGenerationEU/PRTR.

Appendix A. Supplementary data

Supplementary data to this article can be found online at https://doi.org/10.1016/j.molliq.2023.123933.

References

[1] A. Hassan, S.Z. Ilyas, A. Jalil, Z. Ullah, Monetization of the environmental damage caused by fossil fuels, Environ. Sci. Pollut. Res. 28 (2021) 21204–21211, https://doi.org/10.1007/s11356-020-12205-w.
[2] V. Masson-Delmotte, P. Zhai, A. Pirani, S.L. Connors, C. Péan, S. Berger, N. Caud, Y. Chen, L. Goldfarb, M.I. Gomis, eds., IPCC special report on impacts of global warming of 1.5°C above pre-industrial levels in context of strengthening response to climate change, sustainable development, and efforts to eradicate poverty, Cambridge University Press, Cambrigde, UK, 2021. https://www.cambridge.org/core/product/identifier/9781009157940%23prf2/type/book_part.
[3] A. De Gracia, L.F. Cabeza, Phase change materials and thermal energy storage for buildings, Energy Build. 103 (2015) 414–419, https://doi.org/10.1016/j.enbuild.2015.06.007.
[4] L.F. Cabeza, A. Castell, C. Barreneche, A. De Gracia, A.I. Fernández, Materials used as PCM in thermal energy storage in buildings: A review, Renew. Sustain. Energy Rev. 15 (2011) 1675–1695, https://doi.org/10.1016/j.rser.2010.11.018.
[5] G. Ferrer, C. Barreneche, A. Solé, J.E. Juliá, L.F. Cabeza, Recent patents on nano-enhanced materials for use in thermal energy storage (TES), Recent Pat. Nanotechnol. 11 (2017) 101–108.
[6] L.F. Cabeza, Recent advancements in materials and systems for thermal energy storage, 1st Ed., Springer International Publishing, New York, USA, 2019. https://doi.org/10.1007/978-3-319-96640-3.
[7] N.H.S. Tay, M. Liu, M. Belusko, F. Bruno, Review on transportable phase change material in thermal energy storage systems, Renew. Sustain. Energy Rev. 75 (2017) 264–277, https://doi.org/10.1016/j.rser.2016.10.069.
[8] J. Cao, J. Feng, X. Fang, Z. Ling, Z. Zhang, A delayed cooling system coupling composite phase change material and nano phase change material emulsion, Appl. Therm. Eng. 191 (2021) 116888, https://doi.org/10.1016/j.applthermaleng.2021.116888.
[9] M. Delgado, A. Lázaro, J. Mazo, B. Zalba, Review on phase change material emulsions and microencapsulated phase change material slurries: Materials, heat transfer studies and applications, Renew. Sustain. Energy Rev. 16 (2012) 253–273, https://doi.org/10.1016/j.rser.2011.07.152.
[10] L. Liu, J. Niu, J.Y. Wu, Ultrasonication for preparing high-performance phase change material nano-emulsions: Optimization and characterization, J. Mol. Liq. 380 (2023) 121776, https://doi.org/10.1016/j.molliq.2023.121776.
[11] F. Wang, W. Lin, Z. Ling, X. Fang, A comprehensive review on phase change material emulsions: Fabrication, characteristics, and heat transfer performance, Sol. Energy Mater. Sol. Cells. 191 (2019) 218–234, https://doi.org/10.1016/j.solmat.2018.11.016.
[12] C.J. Ho, S.T. Hsu, T.F. Yang, B.L. Chen, S. Rashidi, W.M. Yan, Cooling performance of mini-channel heat sink with water-based nano-PCM emulsion. An experimental study, Int. J. Therm. Sci. 164 (2021) 106903, https://doi.org/10.1016/j.ijthermalsci.2021.106903.
[13] J. Feng, Y. Guo, Z. Ling, X. Fang, Z. Zhang, Performance enhancement and dual-phase change heat transfer mechanism for latent heat storage system using phase change nanoemulsion, Chem. Eng. Sci. 276 (2023) 118827, https://doi.org/10.1016/j.ces.2023.118827.
[14] J. Shao, J. Darkwa, G. Kokogiannakis, Review of phase change emulsions (PCMEs) and their applications in HVAC systems, Energy Build. 94 (2015) 200–217, https://doi.org/10.1016/j.enbuild.2015.03.003.
[15] L. Liu, X. Zhang, H. Liang, J. Niu, J.Y. Wu, Cooling storage performance of a novel phase change material nano-emulsion for room air-conditioning in a self-designed pilot thermal storage unit, Appl. Energy. 308 (2022) 118405, https://doi.org/10.1016/j.apenergy.2021.118405.
[16] V. Vasile, H. Necula, A. Badea, R. Revellin, J. Bonjour, P. Haberschill, Experimental study of the heat transfer characteristics of a paraffin-in-water emulsion used as a secondary refrigerant, Int. J. Refrig. 88 (2018) 1–7, https://doi.org/10.1016/j.ijrefrig.2017.11.029.
[17] T. Morimoto, K. Suzuki, H. Kumano, Heat transfer characteristics of phase change emulsions with solidification of phase change material particles in a circular tube, Int. J. Refrig. 114 (2020) 1–9, https://doi.org/10.1016/j.ijrefrig.2020.02.022.
[18] C. Delgado-Sánchez, A.A. Cuadri, F.J. Navarro, P. Partal, Formulation and processing of novel non-aqueous polyethylene glycol-in-silicone oil (o/o) phase change emulsions, Sol. Energy Mater. Sol. Cells. 221 (2021) 110898, https://doi.org/10.1016/j.solmat.2020.110898.

[19] D. Cabaleiro, F. Agresti, S. Barison, M.A. Marcos, J.I. Prado, S. Rossi, S. Bobbo, L. Fedele, Development of paraffinic phase change material nanoemulsions for thermal energy storage and transport in low-temperature applications, Appl. Therm. Eng. 159 (2019) 113868, https://doi.org/10.1016/j.applthermaleng.2019.113868.
[20] T. Morimoto, M. Sugiyama, H. Kumano, Experimental study of heat transfer characteristics of phase change material emulsions in a horizontal circular tube, Appl. Therm. Eng. 188 (2021) 116634, https://doi.org/10.1016/j.applthermaleng.2021.116634.
[21] D. Cabaleiro, S. Hamze, F. Agresti, P. Estellé, S. Barison, L. Fedele, S. Bobbo, Dynamic viscosity, surface tension and wetting behavior studies of paraffin–in–water nano–emulsions, Energies. 12 (2019) 3334, https://doi.org/10.3390/en12173334.
[22] S. Rashidi, N. Karimi, G. Li, B. Sunden, Progress in phase change nano-emulsions for energy applications. A concise review, J. Mol. Liq. 387 (2023) 122547, https://doi.org/10.1016/j.molliq.2023.122547.
[23] P. O'Neill, L. Fischer, R. Revellin, J. Bonjour, Phase change dispersions: A literature review on their thermo-rheological performance for cooling applications, Appl. Therm. Eng. 192 (2021) 116920, https://doi.org/10.1016/j.applthermaleng.2021.116920.
[24] T. Morimoto, H. Kumano, Flow and heat transfer characteristics of phase change emulsions in a circular tube: Part 1. Laminar flow, Int. J. Heat Mass Transf. 117 (2018) 887–895, https://doi.org/10.1016/j.ijheatmasstransfer.2017.10.055.
[25] F. Wang, X. Fang, Z. Zhang, Preparation of phase change material emulsions with good stability and little supercooling by using a mixed polymeric emulsifier for thermal energy storage, Sol. Energy Mater. Sol. Cells. 176 (2018) 381–390, https://doi.org/10.1016/j.solmat.2017.10.025.
[26] X. Zhang, J.Y. Wu, J. Niu, PCM-in-water emulsion for solar thermal applications: The effects of emulsifiers and emulsification conditions on thermal performance, stability and rheology characteristics, Sol. Energy Mater. Sol. Cells. 147 (2016) 211–224, https://doi.org/10.1016/j.solmat.2015.12.022.
[27] L. Liu, J. Niu, J.Y. Wu, Development of highly stable paraffin wax/water phase change material nano-emulsions as potential coolants for thermal management, Sol. Energy Mater. Sol. Cells. 252 (2023) 112184, https://doi.org/10.1016/j.solmat.2023.112184.
[28] F. Agresti, D. Cabaleiro, L. Fedele, S. Rossi, S. Barison, PMMA nano-encapsulated phase change material colloids for heat management applications, J. Mol. Liq. 377 (2023) 121576, https://doi.org/10.1016/j.molliq.2023.121576.
[29] L. Huang, E. Günther, C. Doetsch, H. Mehling, Subcooling in PCM emulsions-Part 1: Experimental, Thermochim. Acta. 509 (2010) 93–99, https://doi.org/10.1016/j.tca.2010.06.006.
[30] E. Günther, L. Huang, H. Mehling, C. Dötsch, Subcooling in PCM emulsions-Part 2: Interpretation in terms of nucleation theory, Thermochim. Acta. 522 (2011) 199–204, https://doi.org/10.1016/j.tca.2011.04.027.
[31] C.J. Ho, S.C. Chen, C.M. Lai, Experimental study on concentration effects on the supercooling of phase change material-in-water nanoemulsions, Heat Transf. Eng. 44 (2023) 1108–1120, https://doi.org/10.1080/01457632.2022.2119921.
[32] D. Cabaleiro, F. Agresti, L. Fedele, S. Barison, C. Hermida-Merino, S. Losada-Barreiro, S. Bobbo, M.M. Piñeiro, Review on phase change material emulsions for advanced thermal management: Design, characterization and thermal performance, Renew. Sustain. Energy Rev. 159 (2022) 112238, https://doi.org/10.1016/j.rser.2022.112238.
[33] T. Morimoto, H. Kumano, Nucleation promoting effect of fat shell on phase change material particles dispersed in an emulsion for thermal energy storage medium, J. Energy Storage. 31 (2020) 101637, https://doi.org/10.1016/j.est.2020.101637.
[34] L. Liu, J. Niu, J.Y. Wu, Formulation of highly stable PCM nano-emulsions with reduced supercooling for thermal energy storage using surfactant mixtures, Sol. Energy Mater. Sol. Cells. 223 (2021) 110983, https://doi.org/10.1016/j.solmat.2021.110983.
[35] T. Sakai, Y. Nakagawa, K. Iijima, Hexadecane-in-water emulsions as thermal-energy storage and heat transfer fluids: Connections between phase-transition temperature and period of hexadecane droplets dispersed in hexadecane-in-water emulsions and characteristics of surfactants, Colloids Surfaces A Physicochem. Eng. Asp. 529 (2017) 394–402, https://doi.org/10.1016/j.colsurfa.2017.06.015.
[36] G. Hagelstein, S. Gschwander, Reduction of supercooling in paraffin phase change slurry by polyvinyl alcohol, Int. J. Refrig. 84 (2017) 67–75, https://doi.org/10.1016/j.ijrefrig.2017.08.016.
[37] X. Zhang, J. Niu, J.Y. Wu, Evaluation and manipulation of the key emulsification factors toward highly stable PCM-water nano-emulsions for thermal energy storage, Sol. Energy Mater. Sol. Cells. 219 (2021) 110820, https://doi.org/10.1016/j.solmat.2020.110820.
[38] D. Cabaleiro, S. Losada-barreiro, F. Agresti, C. Hermida-merino, L. Fedele, L. Lugo, S. Barison, M.M. Piñeiro, Development and thermophysical profile of alcohol-in-water nanoemulsions for thermal management, Fluids. 7 (2022) 11, https://doi.org/10.3390/fluids7010011.
[39] S. Barison, D. Cabaleiro, S. Rossi, A. Kovtun, M. Melucci, F. Agresti, Paraffin–graphene oxide hybrid nano emulsions for thermal management systems, Colloids Surfaces A Physicochem. Eng. Asp. 627 (2021) 127132, https://doi.org/10.1016/j.colsurfa.2021.127132.
[40] J. Burgos, R. Mondragón, R. Martínez-Cuenca, U. Nithiyanantham, S. Barison, S. Mancin, F. Fabregat-Santiago, L. Hernández, Photothermal properties and performance of hybrid carbon-paraffin/water emulsions, J. Energy Storage. 73 (2023), https://doi.org/10.1016/j.est.2023.109136.
[41] X. Zhang, J. Niu, J.Y. Wu, Development and characterization of novel and stable silicon nanoparticles-embedded PCM-in-water emulsions for thermal energy storage, Appl. Energy. 238 (2019) 1407–1416, https://doi.org/10.1016/j.apenergy.2019.01.159.
[42] Q. Zhao, W. Yang, H. Zhang, F. He, H. Yan, R. He, K. Zhang, J. Fan, Graphene oxide Pickering phase change material emulsions with high thermal conductivity and photo-thermal performance for thermal energy management, Colloids Surfaces A Physicochem. Eng. Asp. 575 (2019) 42–49, https://doi.org/10.1016/j.colsurfa.2019.05.007.
[43] C.J. Ho, K.H. Lin, S. Rashidi, D. Toghraie, W.M. Yan, Experimental study on thermophysical properties of water-based nanoemulsion of *n*-eicosane PCM, J. Mol. Liq. 321 (2021) 114760, https://doi.org/10.1016/j.molliq.2020.114760.
[44] L.J. Fischer, S. von Arx, U. Wechsler, S. Züst, J. Worlitschek, Phase change dispersion properties, modeling apparent heat capacity, Int. J. Refrig. 74 (2017) 240–253, https://doi.org/10.1016/j.ijrefrig.2016.10.008.
[45] P. O'Neill, L. Fischer, P. Haberschill, R. Revellin, J. Bonjour, Heat transfer and rheological performance of a phase change dispersion during crystallisation, Appl. Therm. Eng. 225 (2023) 120139, https://doi.org/10.1016/j.applthermaleng.2023.120139.
[46] S. Puupponen, A. Seppälä, O. Vartia, K. Saari, T. Ala-Nissilä, Preparation of paraffin and fatty acid phase changing nanoemulsions for heat transfer, Thermochim. Acta. 601 (2015) 33–38, https://doi.org/10.1016/j.tca.2014.12.020.
[47] O. Okogeri, V.N. Stathopoulos, What about greener phase change materials? A review on biobased phase change materials for thermal energy storage applications, Int. J. Thermofluids. 10 (2021) 100081, https://doi.org/10.1016/j.ijft.2021.100081.
[48] M.C. Floros, S.S. Narine, Latent heat storage using renewable saturated diesters as phase change materials, Energy. 115 (2016) 924–930, https://doi.org/10.1016/j.energy.2016.09.085.
[49] D. Li, B. Zhuang, Y. Chen, B. Li, V. Landry, A. Kaboorani, Z. Wu, X.A. Wang, Incorporation technology of bio-based phase change materials for building envelope: A review, Energy Build. 260 (2022) 111920, https://doi.org/10.1016/j.enbuild.2022.111920.
[50] N.F.M. Branco, A.I.M.C. Lobo Ferreira, J.C. Ribeiro, L.M.N.B.F. Santos, J.A. P. Coutinho, Understanding the thermal behaviour of blends of biodiesel and diesel: Phase behaviour of binary mixtures of alkanes and FAMEs, Fuel. 262 (2020) 116488.
[51] C. Hu, L. Sha, C. Huang, W. Luo, B. Li, H. Huang, C. Xu, K. Zhang, Phase change materials in food: Phase change temperature, environmental friendliness, and systematization, Trends Food Sci. Technol. 140 (2023) 104167, https://doi.org/10.1016/j.tifs.2023.104167.
[52] C. Delgado-Sánchez, P. Partal, M.J. Martín-Alfonso, F.J. Navarro, Oil-in-Oil emulsions of stearic acid dispersed in silicone oil with enhanced energy storage capability for heat transfer fluids, Sol. Energy Mater. Sol. Cells. 245 (2022) 111893, https://doi.org/10.1016/j.solmat.2022.111893.
[53] F. Wang, J. Guo, S. Li, Y. Wang, Y. Cai, Z. Li, Y. Shen, C. Li, Self-assembly of MXene-decorated stearic acid/ionic liquid phase change material emulsion for effective photo-thermal conversion and storage, Ceram. Int. 49 (2023) 480–488, https://doi.org/10.1016/j.ceramint.2022.09.015.
[54] R. Ravotti, O. Fellmann, N. Lardon, L.J. Fischer, A. Stamatiou, J. Worlitschek, Analysis of bio-based fatty esters PCM's thermal properties and investigation of trends in relation to chemical structures, Appl. Sci. 9 (2019) 225, https://doi.org/10.3390/app9020225.
[55] G. Ferrer, A. Solé, C. Barreneche, I. Martorell, L.F. Cabeza, Corrosion of metal containers for use in PCM energy storage, Renew. Energy. 76 (2015) 465–469, https://doi.org/10.1016/j.renene.2014.11.036.
[56] G. Simonsen, R. Ravotti, P. O'Neill, A. Stamatiou, Biobased phase change materials in energy storage and thermal management technologies, Renew. Sustain. Energy Rev. 184 (2023) 113546, https://doi.org/10.1016/j.rser.2023.113546.
[57] L. Fischer, E. Mura, P. O'Neill, S. von Arx, J. Worlitschek, G. Qiao, Q. Li, Y. Ding, Thermophysical properties of a phase change dispersion for cooling around 50 °C, Int. J. Refrig. 119 (2020) 410–419, https://doi.org/10.1016/j.ijrefrig.2020.05.013.
[58] L. Fischer, E. Mura, P.O. Neill, S. Von Arx, J. Worlitschek, G. Qiao, Q. Li, Y. Ding, Heat transfer performance potential with a high-temperature phase change dispersion, Energies. 14 (2021) 4899, https://doi.org/10.3390/en14164899.
[59] ANSI/ASHRAE Standard 55-2010. Thermal Environmental Conditions for Human Occupancy American Society of Heating, Refrigerating and Air-Co55-2010, ANSI/ASHRAE Standardnditioning Engineers, Atlanta, USA, 2010.
[60] L. Huang, M. Petermann, C. Doetsch, Evaluation of paraffin/water emulsion as a phase change slurry for cooling applications, Energy. 34 (2009) 1145–1155, https://doi.org/10.1016/j.energy.2009.03.016.
[61] M. Kenisarin, K. Mahkamov, Passive thermal control in residential buildings using phase change materials, Renew. Sustain. Energy Rev. 55 (2016) 371–398, https://doi.org/10.1016/j.rser.2015.10.128.
[62] A. Sari, A. Karaipekli, Fatty acid esters-based composite phase change materials for thermal energy storage in buildings, Appl. Therm. Eng. 37 (2012) 208–216, https://doi.org/10.1016/j.applthermaleng.2011.11.017.
[63] Z. Du, C. Wang, X. Tai, G. Wang, X. Liu, Optimization and characterization of biocompatible oil-in-water nanoemulsion for pesticide delivery, ACS Sustain. Chem. Eng. 4 (2016) 983–991, https://doi.org/10.1021/acssuschemeng.5b01058.
[64] W. Wang, H. Wei, Z. Du, X. Tai, G. Wang, Formation and characterization of fully dilutable microemulsion with fatty acid methyl esters as oil phase, ACS Sustain. Chem. Eng. 3 (2015) 443–450, https://doi.org/10.1021/sc500667n.
[65] F. Agresti, L. Fedele, S. Rossi, D. Cabaleiro, S. Bobbo, G. Ischia, S. Barison, Nano-encapsulated PCM emulsions prepared by a solvent-assisted method for solar applications, Sol. Energy Mater. Sol. Cells. 194 (2019) 268–275, https://doi.org/10.1016/j.solmat.2019.02.021.

[66] Q. Gu, C. Bravo-Díaz, L.S. Romsted, Using the pseudophase kinetic model to interpret chemical reactivity in ionic emulsions: Determining antioxidant partition constants and interfacial rate constants, J. Colloid Interface Sci. 400 (2013) 41–48, https://doi.org/10.1016/j.jcis.2013.02.024.
[67] L. Fedele, L. Colla, S. Bobbo, S. Barison, F. Agresti, Experimental stability analysis of different water-based nanofluids, Nanoscale Res. Lett. 6 (2011) 300, https://doi.org/10.1186/1556-276X-6-300.
[68] D. Cabaleiro, C. Gracia-Fernández, L. Lugo, (Solid + liquid) phase equilibria and heat capacity of (diphenyl ether + biphenyl) mixtures used as thermal energy storage materials, J. Chem. Thermodyn. 74 (2014) 43–50, https://doi.org/10.1016/j.jct.2014.03.029.
[69] J.I. Prado, U. Calviño, L. Lugo, Experimental methodology to determine thermal conductivity of nanofluids by using a commercial transient hot-wire device, Appl. Sci. 12 (2022) 329, https://doi.org/10.3390/app12010329.
[70] J. Vijande, M.M. Piñeiro, J. García, J.L. Valencia, J.L. Legido, Density and surface tension variation with temperature for heptane + 1-alkanol, J. Chem. Eng. Data. 51 (2006) 1778–1782, https://doi.org/10.1021/je060179e.
[71] T.F. Tadros, Rheology of dispersions, Wiley-VCH Verlag GmbH & Co. KGaA, Weinheim, Germany, 2010. https://doi.org/10.1002/9783527631568.
[72] C.N. Lunardi, A.J. Gomes, F.S. Rocha, J. De Tommaso, G.S. Patience, Experimental methods in chemical engineering: Zeta potential, Can. J. Chem. Eng. 99 (2021) 627–639, https://doi.org/10.1002/cjce.23914.
[73] M.C. Costa, L.A.D. Boros, J.A.P. Coutinho, M.A. Krähenbühl, A.J.A. Meirelles, Low-temperature behavior of biodiesel: Solid-liquid phase diagrams of binary mixtures composed of fatty acid methyl esters, Energy and Fuels. 25 (2011) 3244–3250, https://doi.org/10.1021/ef2004199.
[74] S. Gahlyan, S. Maken, S.J. Park, Measurement and modelling of solid-liquid equilibria, density and viscosity of fatty acid methyl or ethyl esters, J. Mol. Liq. 314 (2020) 113628, https://doi.org/10.1016/j.molliq.2020.113628.
[75] W.E. Acree, Thermodynamic properties of organic compounds. Part 4. First update of enthalpy of fusion and melting point temperature compilation, Thermochim. Acta. 219 (1993) 97–104.
[76] M.D. Robustillo, L.C.B.A. Bessa, A.J.d.A. Meirelles, P.d.A. Pessôa Filho, Experimental data and thermodynamic modeling of solid-liquid equilibrium of binary systems containing representative compounds of biodiesel and fossil fuels: Ethyl esters and *n*-hexadecane, Fuel. 220 (2018) 303–317.
[77] G.G. Lobbia, G. Berchiesi, G. Vitali, Crystallization curve of hexadecane in mixtures with methyl nonadecanoate, methyl octadecanoate, ethyl octadecanoate, and methyl hexadecanoate. A comparison of the experimental and calculated curves, Thermochim. Acta. 65 (1983) 29–33, https://doi.org/10.1016/0040-6031(83)80004-5.
[78] L. Huang, P. Noeres, M. Petermann, C. Doetsch, Experimental study on heat capacity of paraffin/water phase change emulsion, Energy Convers. Manag. 51 (2010) 1264–1269, https://doi.org/10.1016/j.enconman.2009.12.038.
[79] E.W. Lemmon, M.L. Huber, M.O. McLinden, NIST Standard Reference Database: Reference Fluid Thermodynamic and Transport Properties (REFPROP). Physical and Chemical Properties, Physical and Chemical Properties Division National Institute of Standards and Technology, Boulder, Colorado, 2013.
[80] M.J. van Bommel, H.A.J. Oonk, J.C. van Miltenburg, Heat capacity measurements of 13 methyl esters of *n*-carboxylic acids from methyl octanoate to methyl eicosanoate between 5 K and 350 K, J. Chem. Eng. Data. 49 (2004) 1036–1042, https://doi.org/10.1021/je0499364.
[81] M. Habrioux, J.P. Bazile, G. Galliero, J.L. Daridon, Viscosities of fatty acid methyl and ethyl esters under high pressure: methyl myristate and ethyl myristate, J. Chem. Eng. Data. 61 (2016) 398–403, https://doi.org/10.1021/acs.jced.5b00612.
[82] C. Delgado-Sánchez, P. Partal, M.J. Martín-Alfonso, F.J. Navarro, Role of crystallinity on the thermal and viscous behaviour of polyethylene glycol-in-silicone oil (o/o) phase change emulsions, J. Ind. Eng. Chem. 103 (2021) 348–357, https://doi.org/10.1016/j.jiec.2021.08.003.
[83] H. McPhee, V. Soni, S. Saber, M. Zargartalebi, J. Riordon, M. Holmes, M. Toews, D. Sinton, Rheological behavior of phase change slurries for thermal energy applications, Langmuir. 39 (2023) 129–141, https://doi.org/10.1021/acs.langmuir.2c02279.
[84] X. Zhang, J. Niu, S. Zhang, J.Y. Wu, PCM in water emulsions: Supercooling reduction effects of nano-additives, viscosity effects of surfactants and stability, Adv. Eng. Mater. 17 (2015) 181–188, https://doi.org/10.1002/adem.201300575.
[85] K. Dutkowski, J.J. Fiuk, Experimental investigation of the effects of mass fraction and temperature on the viscosity of microencapsulated PCM slurry, Int. J. Heat Mass Transf. 126 (2018) 390–399, https://doi.org/10.1016/j.ijheatmasstransfer.2018.05.158.
[86] X. Zheng, A. Huang, Y. Bao, S. Wang, G. Qin, Y. Liu, Measurement of the thermal conductivity of the components of biodiesels: Methyl laurate and methyl myristate, Fluid Phase Equilib. 556 (2022) 113409, https://doi.org/10.1016/j.fluid.2022.113409.
[87] J. Fan, P. Liu, Q. Meng, C. Gao, F. Song, Experiment investigation on the liquid thermal conductivity of biodiesel + diesel fuel blends, J. Chem. Eng. Data. 66 (2021) 2597–2605, https://doi.org/10.1021/acs.jced.1c00185.
[88] S. Wi, J. Seo, S.G. Jeong, S.J. Chang, Y. Kang, S. Kim, Thermal properties of shape-stabilized phase change materials using fatty acid ester and exfoliated graphite nanoplatelets for saving energy in buildings, Sol. Energy Mater. Sol. Cells. 143 (2015) 168–173, https://doi.org/10.1016/j.solmat.2015.06.040.
[89] J.C. Maxwell, A treatise on electricity and magnetism, 3rd Ed., Oxford University Press, London, United Kingdom, 1882.
[90] Z. Hashin, S. Shtrikman, A Variational approach to the theory of the effective magnetic permeability of multiphase materials, J. Appl. Phys. 33 (1962) 3125–3131. https://doi.org/10.1063/1.1728579.
[91] T. Morimoto, K. Togashi, H. Kumano, H. Hong, Thermophysical properties of phase change emulsions prepared by D-phase emulsification, Energy Convers. Manag. 122 (2016) 215–222, https://doi.org/10.1016/j.enconman.2016.05.065.
[92] S. Saarinen, S. Puupponen, A. Meriläinen, A. Joneidi, A. Seppälä, K. Saari, T. Ala-Nissila, Turbulent heat transfer characteristics in a circular tube and thermal properties of *n*-decane-in-water nanoemulsion fluids and micelles-in-water fluids, Int. J. Heat Mass Transf. 81 (2015) 246–251, https://doi.org/10.1016/j.ijheatmasstransfer.2014.10.029.
[93] M.J. Pratas, S. Freitas, M.B. Oliveira, S.C. Monteiro, Á.S. Lima, J.A.P. Coutinho, Densities and viscosities of minority fatty acid methyl and ethyl esters present in biodiesel, J. Chem. Eng. Data. 56 (2011) 2175–2180, https://doi.org/10.1021/je1012235.
[94] C.J. Ho, J.B. Huang, P.S. Tsai, Y.M. Yang, Preparation and properties of hybrid water-based suspension of Al_2O_3 nanoparticles and MEPCM particles as functional forced convection fluid, Int. Commun. Heat Mass Transf. 37 (2010) 490–494, https://doi.org/10.1016/j.icheatmasstransfer.2009.12.007.